Chemical Engineering Journal 469 (2023) 144010

Contents lists available at ScienceDirect

Chemical Engineering Journal

journal homepage: www.elsevier.com/locate/cej

Frequency-tunable and absorption/transmission-switchable microwave absorber based on a chitin-nanofiber-derived elastic carbon aerogel

Xiang Li, Luting Zhu, Takaaki Kasuga, Masaya Nogi, Hirotaka Koga *

SANKEN (The Institute of Scientific and Industrial Research), Osaka University, 8-1 Mihogaoka, Ibaraki, Osaka 567-0047, Japan

ARTICLE INFO

Keywords:
Chitin nanofiber
Elastic carbon aerogel
Microwave absorption
Absorption frequency tuning
Absorption/transmission switching

ABSTRACT

The increasing use of microwaves in wireless communications has caused severe electromagnetic pollution. As the frequency range for wireless communication is expanding, it is highly desirable to develop a microwave absorber that can smartly and reversibly tune its absorption and transmission properties on demand to transmit required frequencies and absorb unwanted frequencies. Herein, an absorption-frequency-tunable and absorption/transmission-switchable microwave absorber is developed based on the controlled compression of a chitin-derived elastic carbon aerogel. The maximum absorption frequency is tuned from 10.4 to 11.0, 11.5, and 12.1 GHz by varying the compression strain from 0 to 20, 40, and 60%, respectively, while the maximum absorption intensity is maintained at approximately −40 dB. This frequency-tunable absorption is achieved by reducing the thickness of the carbon aerogel while retaining its moderate dielectric loss tangent. Further compression from 60 to 80% switches the carbon aerogel from being a microwave absorber to transmitter while causing impedance mismatch and changing its dielectric loss tangent from moderate to low levels. The frequency tunability and microwave absorption/transmission switching capability are reversible and repeatable for at least 60,000 cycles of compression and recovery. This study provides insights into the smart and reversible control of microwave absorbing properties and paves the way for multifunctional and robust absorbers.

1. Introduction

Electromagnetic waves are used for wireless transmission of information [1]. Excessive use of electromagnetic waves can interfere with the operation of precision instruments and induce adverse effects on human health [2]. Microwave absorbers have been intensively developed to reduce electromagnetic pollution [3]. Because the frequency range of electromagnetic waves used for wireless communication is expanding, it is highly desirable to develop a microwave absorber that can smartly tune its absorption frequency and absorption/transmission properties to meet the specific application requirements and/or real-time environmental changes [4]. Sufficient impedance matching between the microwave absorber and air is essential to suppress reflection and enhance absorption [5]. To switch between absorption and transmission, the dielectric loss tangent of the microwave absorber should be reportedly tuned [6] because moderate or low dielectric loss tangent can result in microwave absorption or transmission, respectively [7], while a high dielectric loss results in microwave reflection [8].

Ideally, absorption/transmission switching and frequency-tunable absorption should be reversibly achieved using a single microwave absorber. Carbon-aerogel-based microwave absorbers have attracted considerable attention owing to their light weight [9], chemical stability [10], and versatile applications [11]. As a pioneering example, switching from microwave transmission to absorption was recently reported using a carbon black nanoparticle/wood-derived lamellar carbon aerogel [6]. The carbon aerogel exhibited microwave transmission in its original state because of its low dielectric loss tangent. Owing to the elasticity of the carbon aerogel, its dielectric loss tangent could be tuned from low to moderate levels by mechanical compression, enabling a switching from transmission to absorption [6]. To the best of our knowledge, frequency-tunable absorption using a single carbon aerogel remains challenging. To overcome this challenge, the carbon aerogel should reversibly change its thickness to modulate its impedance-matched frequency according to the well-established quarter-wavelength theory [12] while retaining its moderate dielectric loss tangent. Despite such theoretical predictions, the dynamic adjustment of the thickness and dielectric loss tangent has seldom been achieved.

In our previous study, a chitin-derived carbon aerogel with

* Corresponding author.
E-mail address: hkoga@eco.sanken.osaka-u.ac.jp (H. Koga).

https://doi.org/10.1016/j.cej.2023.144010
Received 26 February 2023; Received in revised form 26 May 2023; Accepted 6 June 2023
Available online 9 June 2023

anisotropic honeycomb-like porous channels and N- and O-doped defective carbon structures was fabricated, providing a strong microwave absorption performance owing to its good impedance matching and moderate dielectric loss tangent [13]. In this study, the elastic properties of the chitin-derived carbon aerogel microwave absorber were elaborated and applied to achieve absorption-frequency tuning and further absorption/transmission switching (Fig. 1). The chitin-derived carbon aerogel exhibited good elasticity in the direction perpendicular to its anisotropic porous channels. Compressing the carbon aerogel could reduce its thickness while maintaining its good impedance matching and moderate dielectric loss tangent, tuning its maximum absorption frequency in the X-band (8.2–12.4 GHz), which is used for various applications in radar, satellite communication, and wireless computer networks [14]. Further compression of the carbon aerogel causes impedance mismatch and significantly decreases its dielectric loss tangent, switching it from microwave absorption to transmission. Such frequency-tunable and absorption/transmission-switchable feature is reversible and maintained even after 60,000 cycles of compression and recovery, proving smart and robust microwave absorption using a single carbon aerogel.

2. Experimental section

2.1. Materials

A chitin nanofiber/water suspension (BiNFi-s chitin, SFo-20002, Fig. S1) was obtained from Sugino Machine Ltd. (Toyama, Japan). Acrylic plates (thickness = 1 mm) were purchased from Acrysunday Co. Ltd. (Osaka, Japan). Conductive copper foil adhesive tape (No. 8701-00) was purchased from Maxell Sliontec Ltd. (Kanagawa, Japan).

2.2. Fabrication of chitin-derived carbon aerogel

Chitin-derived carbon aerogels were prepared by unidirectional ice templating, freeze-drying, and subsequent carbonization, according to our previous report [13]. Briefly, a chitin nanofiber/water suspension (1.0 wt%, 24 mL) was first defoamed by a centrifugal vacuum apparatus (ARV-930TWIN, Thinky Corp., Tokyo, Japan) at 1,400 rpm for 5 min at room temperature. The resulting suspension was then poured into a handmade acrylic box (40 mm width × 30 mm length × 20 mm depth), where an inner wall (40 mm width × 20 mm depth) was pre-attached using Cu foil adhesive tape. Subsequently, a chitin nanofiber/water suspension-containing acrylic box (with the Cu side) was attached to a liquid N_2-containing cubic open steel box for unidirectional ice templating. After the chitin nanofiber/water suspension was fully frozen, freeze-drying was performed for 60 h to prepare the chitin aerogel (EYELA FDU-2200, Tokyo Rikakikai Co., Ltd., Tokyo, Japan). Finally, the obtained chitin aerogel was carbonized under a N_2 atmosphere in a temperature-programmable muffle furnace (KDF75, Denken-Highdental Co., Ltd., Kyoto, Japan). The temperature was controlled as follows: (1) an increase from room temperature to 500 °C at a heating rate of 2 °C min^{-1} and maintained for 2 h; (2) an increase to 700, 800, or 900 °C at a heating rate of 5 °C min^{-1} and maintained for 1 h; (3) cooling at 2 °C min^{-1} to room temperature.

2.3. Evaluation of elastic properties of a chitin-derived carbon aerogel

The elastic properties of the chitin-derived carbon aerogels were evaluated using a compression testing equipment with a 500-N load cell (EZ-SX, Shimadzu Co., Ltd., Osaka, Japan). The cuboidal carbon aerogel was loaded between the two compression stages and the top stage was responsible for applying the uniaxial compression force and releasing the carbon aerogel. The loading direction was perpendicular to the anisotropic porous channels of the carbon aerogel. All hysteresis curves with maximum strains of 20, 40, 60, and 80% were obtained at a stroke rate of 10 mm min^{-1}. For the compression fatigue resistance measurement during 60,000 cycles of 80% compression and recovery, continuous cyclic compression for the carbon aerogel was performed with a compression frequency of 0.4 Hz by using a Desktop Model Endurance Testing Machine (DLDM111LHB, YUASA System Co., Ltd., Okayama, Japan). The stress retention was calculated as the percentage ratio of the maximum stress value in each cycle to that in the first cycle [15]. The energy loss coefficient was calculated by the percentage ratio of energy loss to the energy storage during cyclic compression, which is represented by the following equation [16]:

$$\text{Energy loss coefficient} = \frac{U''}{U'} \times 100\% \quad (1)$$

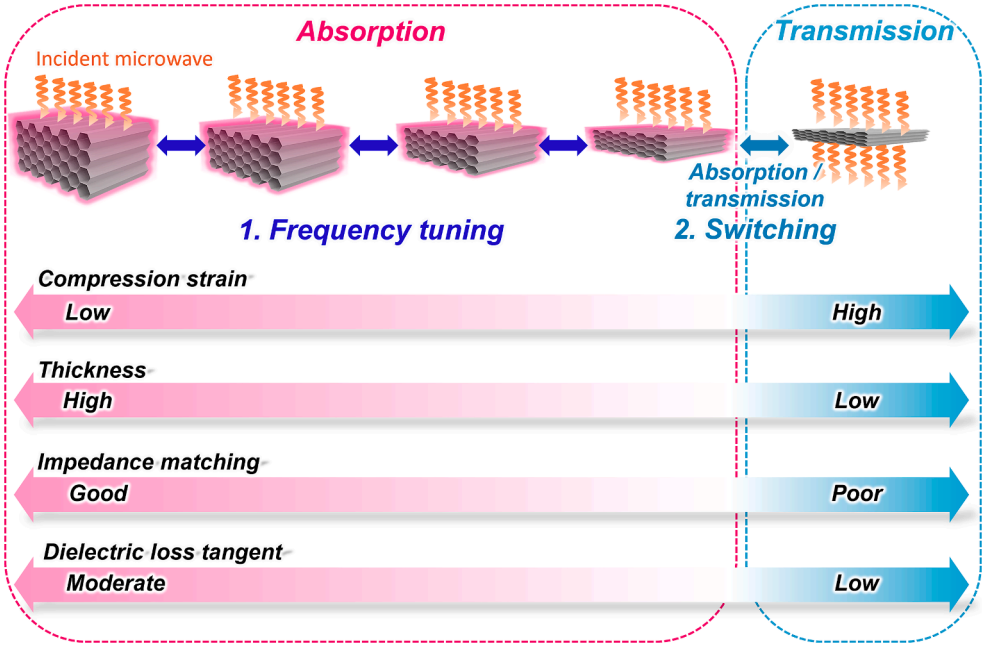

Fig. 1. Schematic of the strategy to tune the absorption frequency and switch from absorption to transmission of the chitin-derived elastic carbon aerogel with anisotropic porous channels by compressing it.

where U'' and U' represent the energy loss and storage in each compression cycle, respectively, which were obtained from the integral area of the stress–strain curve.

2.4. Evaluation of microwave absorption performance, impedance matching, and dielectric loss tangent of a chitin-derived carbon aerogel

The experimental setup is shown in Fig. S2a. The chitin-derived carbon aerogels were cut into cuboidal shapes (23.5 mm width × 10.5 mm length × 6.9 mm thickness) and set into a microwave test fixture (23.5 mm width × 10.5 mm length × 9.7 mm thickness). The thickness of the carbon aerogel was tuned inside the test fixture through mechanical compression in the direction perpendicular to the anisotropic porous channels by sandwiching two microwave-transparent acrylic plates (Fig. S2b, 23.5 mm width × 10.5 mm length × 1.0 mm thickness). The thickness of the compressed carbon aerogel was estimated by considering the depth of the test fixture (9.7 mm), the free space, and the thickness of the acrylic plates (1.0 mm). The electromagnetic parameters of the compressed carbon aerogel at strains of 0, 20, 40, 60, and 80% (thickness: 6.90, 5.52, 4.14, 2.76, and 1.38 mm, respectively), including the complex dielectric permittivity (ε' and ε'') and magnetic permeability (μ' and μ'') versus frequency, were measured using a vector network analyzer (E5071C, Agilent Technologies, Inc., California, USA) with an X-band waveguide test chamber (WR-90, KeyCom Corp, Tokyo, Japan), while the incident microwave radiated from the perpendicular direction to the anisotropic porous channels of the carbon aerogel. The microwave absorption performance was evaluated using the reflection loss (RL) values, which were calculated based on the transmission line theory using the following equations (Eqs. (2) and (3) [17–18]:

$$RL(dB) = 20\log_{10}\left|\frac{Z_{in}-1}{Z_{in}+1}\right| \tag{2}$$

$$Z_{in} = \sqrt{\frac{\mu_r}{\varepsilon_r}}\tanh\left[j\left(\frac{2\pi fd}{c}\right)\sqrt{\mu_r\varepsilon_r}\right] \tag{3}$$

where Z_{in} is the input impedance, ε_r and μ_r are the dielectric permittivity ($\varepsilon_r = \varepsilon'+j\varepsilon''$) and magnetic permeability ($\mu_r = \mu'+j\mu''$) of the carbon aerogel, respectively, j accounts for the imaginary unit, f (GHz) is the frequency of the electromagnetic wave, d (m) is the thickness of the carbon aerogel, and c is the velocity of light (3×10^8 m s^{-1}). The RL values of the compressed carbon aerogel were calculated at strains of 0, 20, 40, 60, and 80% (thickness: 6.90, 5.52, 4.14, 2.76, and 1.38 mm, respectively). The impedance matching values ($|Z_{in}–1|$) of the carbon aerogel were calculated using the modulus of Z_{in}–1 [19–20]. Dielectric loss tangent values were calculated by dividing the imaginary part to the real part of complex permittivity ($\varepsilon''/\varepsilon'$) [21].

2.5. Evaluation of capacitance and electrical conductivity of a chitin-derived carbon aerogel under AC

While the incident microwave was radiated along the direction perpendicular to the anisotropic porous channels of the carbon aerogel, its AC capacitance and AC electrical conductivity along this direction versus frequency were calculated by the following equations (Eqs. (4) [22] and (5) [23]):

$$C = \frac{\varepsilon_0\varepsilon_r A}{d} \tag{4}$$

$$\sigma_{AC} = 2\pi f\varepsilon_0\varepsilon'' \tag{5}$$

where C (F) is the AC capacitance, ε_0 (F m^{-1}) is the dielectric constant of vacuum, ε_r is the dielectric permittivity ($\varepsilon_r = \varepsilon'+j\varepsilon''$), A (m^2) and d (m) are the area and thickness of the carbon aerogel, respectively, σ_{AC} (S m^{-1}) is the AC electrical conductivity, f (GHz) is the frequency of the electromagnetic wave, and ε'' is the imaginary part of the complex dielectric permittivity of the carbon aerogel.

2.6. Characterization

The morphologies of the carbon aerogels parallel and perpendicular to their porous channels were observed by a field-emission scanning electron microscope (FE-SEM) at an acceleration voltage of 2 kV (SU-8000, Hitachi High-Tech Science Corp., Tokyo, Japan). FE-SEM images were obtained at compression strains of 0, 20, 40, 60, and 80% by compressing the carbon aerogel between two conductive Cu foil adhesive tapes. Prior to FE-SEM observation, the carbon aerogel was subjected to platinum sputtering at 20 mA for 10 s (ION SPUTTER, E-1045, Hitachi High-Tech Science Corp., Tokyo, Japan).

3. Results and discussion

3.1. Fabrication and elastic properties of chitin-derived carbon aerogel

To realize absorption-frequency tuning and absorption/transmission switching by mechanical compression, a chitin-derived carbon aerogel was fabricated based on the workflow shown in Fig. 2a. Starting from the crab-shell-derived chitin nanofiber/water suspension, the carbon aerogel was prepared *via* unidirectional ice templating, freeze-drying, and subsequent carbonization at 800 °C, according to our previous report [13]. The as-fabricated carbon aerogel possessed anisotropic honeycomb-like porous channels (Fig. 2b–e) with thin channel walls consisting of nanofiber networks (inset of Fig. 2e) derived from a unidirectionally grown ice template [24]. The carbon aerogel was free-standing with a very low density (approximately 7.5 mg cm^{-3}).

As shown in Fig. 3a, the carbon aerogel could be compressed to 80% strain in the direction perpendicular to the anisotropic porous channels, and it returned to its original state after unloading (Supporting video S1). To further understand the mechanical properties of the carbon aerogel, the stress–strain curves of the carbon aerogel during compression loading and unloading were recorded upon successive cyclic compression at strains ranging from 0 to 20, 40, 60, and 80% (Fig. 3b). The stress–strain curves of the carbon aerogel were consistent at each cyclic compression. At a strain of 80%, the stress was approximately 50 kPa. It remained above 0 until the strain reached 0% during the unloading process, indicating complete recovery [25]. These results indicated that the carbon aerogel deformed elastically in the direction perpendicular to the anisotropic porous channels up to a compression strain of 80%. Such elastic behavior was, however, not observed when it was compressed along the direction parallel to the anisotropic porous channels (Fig. S3a). On the other hand, the chitin aerogel without carbonization did not deform elastically in either direction (Fig. S3b and c).

To evaluate the compression fatigue resistance, the carbon aerogel was subjected to a cyclic compression with a loading strain of 80%. The elastic properties were maintained even after 60,000 cycles of compression and recovery (Fig. 3c). Although the compression stress at a strain of 80% decreased to approximately 70%, its energy loss coefficient (the ratio of the energy dissipated within the material to the compression energy [26]) remained almost unchanged (Fig. 3d). These results indicated that the compression fatigue-resistance of the carbon aerogel was sufficient for at least 60,000 cycles of compression and recovery. It has been reported that graphene [27,28] and MXene aerogels [29] with anisotropic porous channels also deform elastically upon compression perpendicular to the porous channels. In agreement with this, our chitin-derived carbon aerogel had an anisotropic porous channel structure (Fig. 2b–e), and it could be compressed in the direction perpendicular to that of the channels without obvious fracture at strains ranging from 20 to 80% (Fig. 3e) even after 60,000 cycles of compression and recovery at a strain of 80% (Fig. 3f).

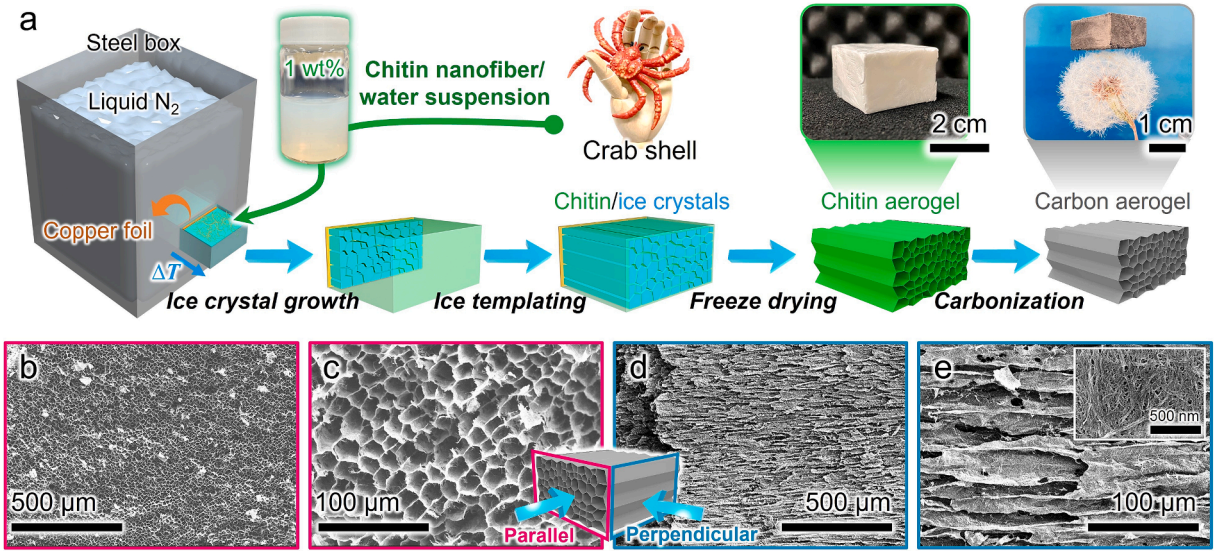

Fig. 2. Preparation and morphology of the chitin-derived carbon aerogel. (a) Schematic of the preparation. FE-SEM images of the carbon aerogel in (b, c) parallel and (d, e) perpendicular direction of the anisotropic honeycomb-like porous channels. Carbonization temperature: 800 °C.

3.2. *Frequency-tunable microwave absorption by chitin-derived elastic carbon aerogel*

The microwave absorption performance of the carbon aerogel in the X-band (8.2–12.4 GHz) was evaluated at different compression strains in the direction perpendicular to the anisotropic porous channels while irradiating along the compression direction. As shown in Fig. 4a, the uncompressed carbon aerogel had a minimum RL (*i.e.*, maximum microwave absorption) of approximately −40 dB at a frequency of 10.4 GHz, which was similar to those of other carbon-based elastic aerogels such as graphene and MXene aerogels reported previously (Table S1). This minimum RL could be maintained by compressing the carbon aerogel from 0 to 20, 40, and 60% strains, with the maximum absorption frequency changing from 10.4 to 11.0, 11.5, and 12.1 GHz, respectively. Thus, the carbon aerogel upon compression from 0 to 60% strain could achieve frequency-tunable absorption in the X-band.

The mechanism of frequency-tunable absorption is discussed next. The observed maximum absorption frequencies (10.4, 11.0, 11.5, and 12.1 GHz) at compression strains of 0, 20, 40, and 60% (respectively) were consistent with the impedance-matched frequencies, wherein the impedance matching values ($|Z_{in}$-1|) were close to zero (Fig. 4b). In the impedance-matched frequency range, absorption is the most effective while reflection usually is suppressed [19,30]. According to the quarter-wavelength theory [12], the impedance-matched frequency tends to increase with decreasing the thickness and dielectric permittivity of the microwave absorber. Upon compressing the elastic carbon aerogel from 0 to 60%, its thickness reduced and dielectric permittivity increased, indicating that thickness reduction plays an important role in increasing the impedance-matched frequency (maximum absorption frequency) of the carbon aerogel (see Fig. S4 for more details). The dielectric loss tangent, which comprises conductive and polarization losses, is also key parameters for the conversion of microwave to heat or other forms of energy, thus affecting the microwave absorption performance [13,31–34]. The excessive, moderate, and low dielectric loss tangent is reportedly related to the reflection, absorption, and transmission of microwaves, respectively [3,35–36]. Although the dielectric loss tangent of the carbon aerogel gradually decreased with increasing compression strain from 0 to 60% (Fig. 4c), its value could be maintained at a moderate level for microwave absorption at the impedance-matched frequency (Fig. 4a). Thus, the carbon aerogel achieved frequency-tunable microwave absorption by reducing its thickness upon compression while maintaining good impedance matching and moderate dielectric loss tangent (Fig. S5a).

Frequency-tunable microwave absorption should be conducted reversibly and repeatedly to satisfy specific application requirements and/or real-time environmental changes. As shown in Fig. 4d and e, the frequencies at the minimum reflection (i.e., the maximum absorption frequencies) and the minimum RL values of the carbon aerogel at compression strains of 0, 20, 40, and 60% remained almost unchanged even after 60,000 cycles of compression and recovery at a strain of 80%. This indicated that the frequency-tunable microwave absorption ability of the carbon aerogel was reversible and repeatable. Such robust frequency-tunable absorption of the carbon aerogel is related to its high compression fatigue resistance (Fig. 3c–f), which retained the impedance matching and dielectric loss tangent even after 60,000 cycles of compression and recovery (Fig. S6).

3.3. *Absorption/transmission-switchable microwave absorption by chitin-derived elastic carbon aerogel*

As shown in Fig. 4a, further compression of the carbon aerogel from 60 to 80% strain resulted in poor microwave absorption performance (RL: more than −10 dB) over the entire X-band. To elaborate the poor microwave absorption of the carbon aerogel at a compression strain of 80%, its reflection, transmission, and absorption coefficient values were calculated, based on the logarithmic ratio of incident power to transmission power [37–40] (Fig. S7). At a compression strain of 80%, the carbon aerogel showed very low reflection coefficient (Fig. S7a, see also Fig. S8), while its transmission coefficient was higher than its absorption coefficient (Fig. S7b and c). These results indicated that the carbon aerogel could allow microwave transmission at a compression strain of 80%. Moreover, the impedance matching value ($|Z_{in}$–1|) of the carbon aerogel increased (Fig. 4b) and its dielectric loss tangent drastically decreased (Fig. 4c). Such impedance mismatch leads to either microwave transmission or reflection [3,41], while low dielectric loss tangent is reportedly related to microwave transmission [36,42]. Thus, the carbon aerogel switched from microwave absorption to transmission in the X-band upon compressing it to 80% strain possibly by causing impedance mismatch and changing its dielectric loss tangent from moderate to low levels (Fig. S5b). The minimum RL values at compression strains of 60 and 80% remained almost unchanged even after 60,000 cycles of compression and recovery (Fig. 4e, see also Fig. S6), indicating that the absorption/transmission switching was reversible and repeatable.

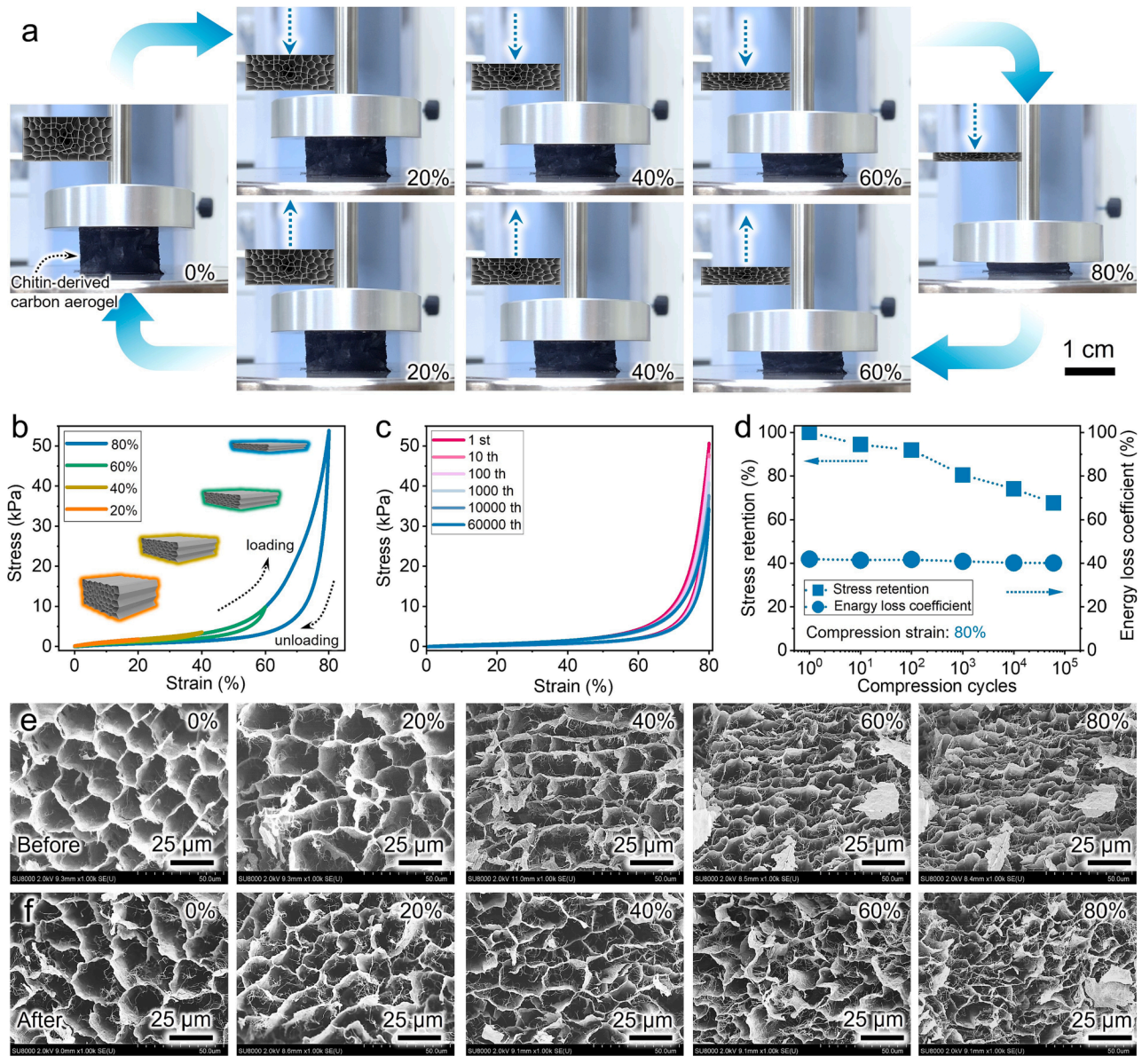

Fig. 3. Elastic properties and compression fatigue resistance in the direction perpendicular to the anisotropic porous channels of the chitin-derived carbon aerogel. (a) Optical images and (b) stress–strain curves of the carbon aerogel during compression loading and unloading with strains of 0 to 20, 40, 60, and 80%. (c) Stress–strain curves and (d) stress retention and energy loss coefficient of the carbon aerogel during 60,000 cycles of compression and recovery at a strain of 80%. Cross-section FE-SEM images in parallel direction of the carbon aerogel at compression strains of 0, 20, 40, 60, and 80% (e) before and (f) after 60,000 cycles of compression and recovery at a strain of 80%. Carbonization temperature: 800 °C.

As described above, the carbon aerogel switched from microwave absorption to transmission upon compressing it to 80% strain, while drastically decreasing its dielectric loss tangent. Because the dielectric loss tangent is expressed as the imaginary part (ε'') divided by the real part (ε') of the complex dielectric permittivity [43], changes in ε' and ε'' of the carbon aerogel upon compression were analyzed to discuss the switching mechanism. The ε' and ε'' of the carbon aerogel increased in a similar way at compression strains from 0 to 60%. In contrast, the ε' showed a much higher increase than ε'' upon further compressing the aerogel to 80% (Fig. 5a and b), drastically decreasing its dielectric loss tangent (Fig. 4c). Theoretically, ε' and ε'' increase with capacitance and electrical conductivity, respectively [44–45]. Therefore, the drastic decrease in dielectric loss tangent ($\varepsilon''/\varepsilon'$) of the carbon aerogel was dominated by the increase in the capacitance rather than the electrical conductivity, although both the capacitance and electrical conductivity increased upon compression from 60 to 80% strain (Fig. 5c and d). This significant increase in the capacitance was mainly due to the increase in its dielectric permittivity as less air remained within the carbon aerogel at a high compression strain, especially at 80% (see Supporting Note 1 for more details).

To realize absorption/transmission switching and absorption-frequency tuning by compression, it is also important to properly tune the impedance matching and dielectric loss tangent of the uncompressed carbon aerogel. In our previous study, the carbonization temperature for the carbon aerogels was controlled to tailor their N- and O-doped defective carbon structures, which largely affected their impedance matching and dielectric loss tangent, and thus microwave absorption performance (Figs. S9 and 10). The carbon aerogel carbonized at 800 °C had the optimized defective carbon structures, providing good impedance matching, moderate dielectric loss tangent, and strong microwave absorption [13]. This carbon aerogel showed frequency-tunable microwave absorption upon compression from 0 to 60% strain and

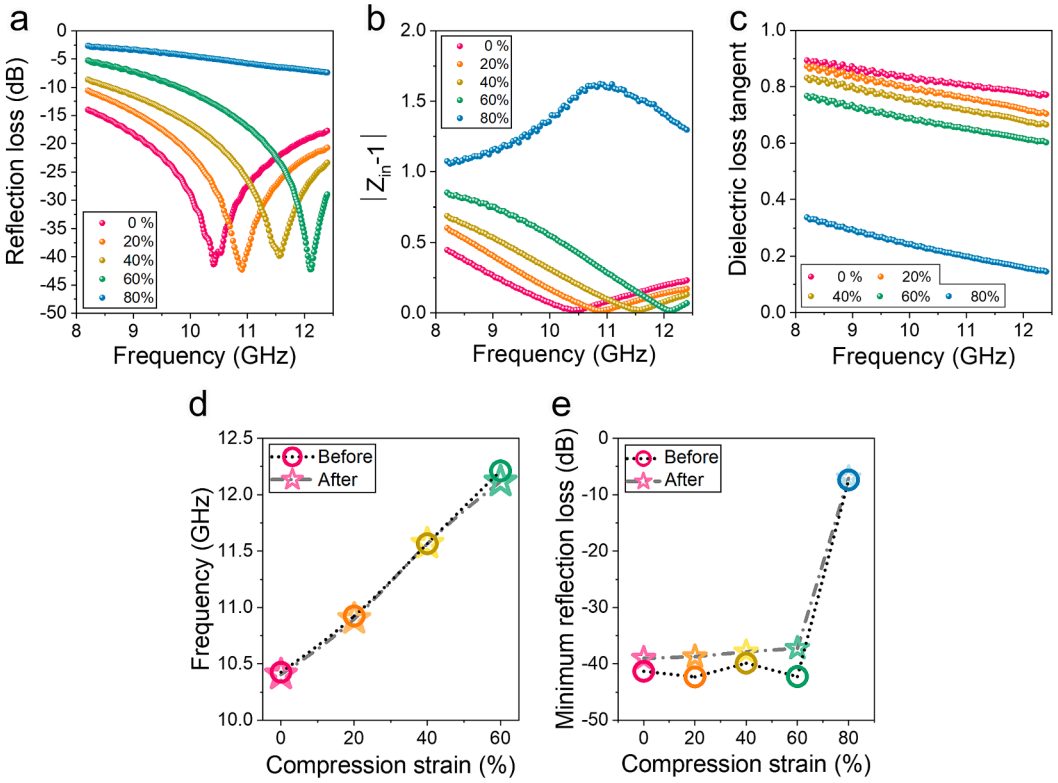

Fig. 4. Frequency-tunable and absorption/transmission-switchable microwave absorption performance of the chitin-derived carbon aerogel upon compression in the perpendicular direction to the anisotropic porous channel. (a) Reflection loss (RL), (b) impedance matching value ($|Z_{in}-1|$), and (c) dielectric loss tangent versus frequency at the compression strain of 0, 20, 40, 60, and 80%. (d) Frequency at the minimum RL of the carbon aerogel at different compression strains, and (e) minimum RL of the carbon aerogel at different compression strains before and after 60,000 cycles of compression and recovery at a strain of 80%. For calculation of the RL, thicknesses of the carbon aerogels were 6.90, 5.52, 4.14, 2.76, and 1.38 mm at compression strains of 0, 20, 40, 60, and 80%, respectively. Carbonization temperature: 800 °C.

absorption/transmission switching at 80% strain. On the other hand, the carbon aerogels carbonized at 700 and 900 °C showed impedance mismatch and had low and excessive dielectric loss tangent, respectively, owing to their inappropriate defective carbon structures. Moreover, their poor microwave absorption performance did not improve with compression (see Fig. S11 for more details). These results indicated that the initial impedance matching and dielectric loss tangent of the carbon aerogel should be set at a good level and a moderate level, respectively. Only then, subsequent compression could allow tuning of the maximum-absorption frequency and switching from the absorption to transmission.

The elastic carbon black nanoparticles/wood-derived lamellar carbon aerogel with low dielectric loss tangent reported previously [6] switched from microwave transmission to absorption upon compression by an increase in the electrical conductivity and ε''. On the other hand, our elastic chitin-derived carbon aerogel with moderate dielectric loss tangent could tune the maximum-absorption frequency by reducing its thickness and maintaining its moderate dielectric loss tangent, while it could switch from absorption to transmission upon further compression by the predominant increase in the capacitance and ε'. The absorption bandwidth in the X-band of the chitin-derived carbon aerogel was 4.2 (8.2–12.4 GHz), 4.2 (8.2–12.4 GHz), 3.8 (8.6–12.4 GHz), 2.6 (9.8–12.4 GHz), and 0 GHz at compression strains of 0, 20, 40, 60, and 80%, respectively (Table S2). Moreover, the chitin-derived carbon aerogel showed poor microwave reflection regardless of its compression strains (Figs. S7 and S8). These results suggest that the microwave absorption properties of the carbon aerogel can be tuned by compression to transmit required frequencies and absorb unwanted frequencies in the X-band (see Table S2 for more details). As chitin is one of the most abundant and renewable biomass materials on Earth, our strategy opens a door for the development of smart and sustainable microwave absorbers.

4. Conclusion

Herein, frequency-tunable microwave absorption and switchable microwave absorption or transmission were successfully demonstrated using a single chitin-derived carbon aerogel. The carbon aerogel with honeycomb-like anisotropic porous channels has good elastic properties and high compression fatigue resistance, allowing mechanical compression and recovery in the direction perpendicular to the porous channels. The uncompressed carbon aerogel showed a maximum microwave absorption of approximately −40 dB at 10.4 GHz, owing to its good impedance matching and moderate dielectric loss tangent. The thickness, impedance matching, and dielectric loss tangent of the carbon aerogel could be tuned by compressing it along the direction perpendicular to the anisotropic porous channels. When the compression strain was varied from 0 to 20, 40, and 60%, the maximum-absorption frequency was observed to vary from 10.4 to 11.0, 11.5, 12.1 GHz, respectively, because the thickness of the carbon aerogel was reduced, and its good impedance matching and moderate dielectric loss tangent were maintained. Furthermore, the carbon aerogel could switch from absorption to transmission when the compression strain increased from 60 to 80% by causing impedance mismatch and changing its dielectric loss tangent from moderate to low levels. Thus, the carbon aerogel achieved frequency-tunable and absorption/transmission-switchable microwave absorption, suggesting its potential applicability as a smart microwave absorber in the X-band. The key to the smart microwave absorption was through the use of the elastic carbon aerogel with good impedance matching and moderate dielectric loss tangent and tuning its

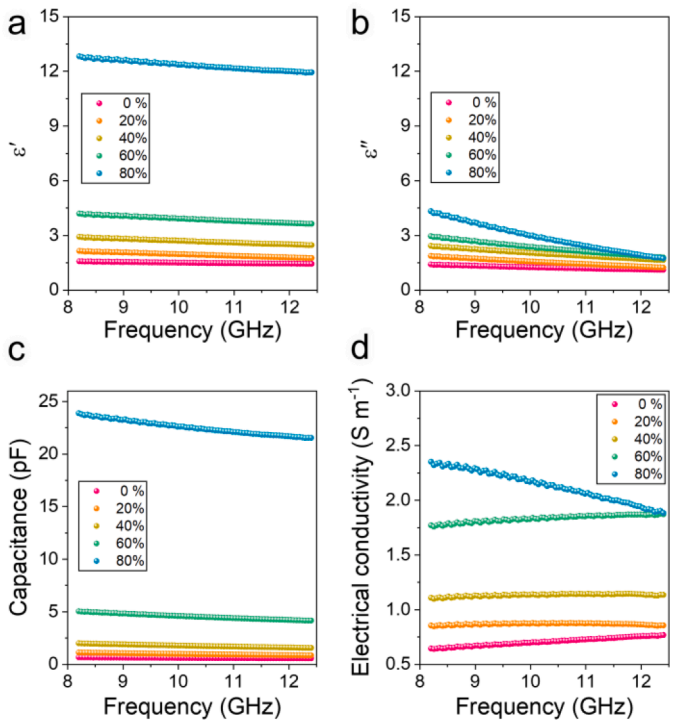

Fig. 5. Change in complex dielectric permittivity, capacitance, and electrical conductivity of the chitin-derived carbon aerogel upon compression in the perpendicular direction to the anisotropic porous channel. (a) Real part (ε'), (b) imaginary part (ε'') of the complex dielectric permittivity, and (c) capacitance and (d) electrical conductivity under alternating current (AC) versus frequency at different compression strains. These values were measured in the same direction as the compression. Carbonization temperature: 800 °C.

thickness, impedance matching, and dielectric loss tangent by controlling the compression. This smart microwave absorption was reversible and repeatable over at least 60,000 cycles of compression and recovery. This study paves the way for the design of a smart and robust microwave absorber that can reversibly tune its properties on demand.

Declaration of Competing Interest

The authors declare that they have no known competing financial interests or personal relationships that could have appeared to influence the work reported in this paper.

Data availability

Data will be made available on request.

Acknowledgements

This work was partially supported by the JST SPRING Program (JPMJSP2138 to X. L.) and JST FOREST Program (JPMJFR2003 to H. K.).

Appendix A. Supplementary data

Supplementary data to this article can be found online at https://doi.org/10.1016/j.cej.2023.144010.

References

[1] T.D.P. Perera, D.N.K. Jayakody, S.K. Sharma, S. Chatzinotas, J. Li, Simultaneous wireless information and power transfer (SWIPT): recent advances and future challenges, IEEE Commun. Surv. Tutorials 20 (2018) 264–302, https://doi.org/10.1109/COMST.2017.2783901.

[2] F. Shahzad, M. Alhabeb, C.B. Hatter, B. Anasori, S.M. Hong, C.M. Koo, Y. Gogotsi, Electromagnetic interference shielding with 2D transition metal carbides (MXenes), Science 353 (2016) 1137–1140, https://doi.org/10.1126/science.aag2421.

[3] F. Meng, H. Wang, F. Huang, Y. Guo, Z. Wang, D. Hui, Z. Zhou, Graphene-based microwave absorbing composites: a review and prospective, Compos. Part B Eng. 137 (2018) 260–277, https://doi.org/10.1016/j.compositesb.2017.11.023.

[4] Z. Cheng, R. Wang, Y. Cao, Z. Cai, Z. Zhang, Y. Huang, Intelligent off/on switchable microwave absorption performance of reduced graphene oxide/VO_2 composite aerogel, Adv. Funct. Mater. 32 (2022) 2205160, https://doi.org/10.1002/adfm.202205160.

[5] F. Ye, Q. Song, Z. Zhang, W. Li, S. Zhang, X. Yin, Y. Zhou, H. Tao, Y. Liu, L. Cheng, L. Zhang, H. Li, Direct growth of edge-rich graphene with tunable dielectric properties in porous Si_3N_4 ceramic for broadband high-performance microwave absorption, Adv. Funct. Mater. 28 (2018) 1707205, https://doi.org/10.1002/adfm.201707205.

[6] X. Liu, Y. Li, X. Sun, W. Tang, G. Deng, Y. Liu, Z. Song, Y. Yu, R. Yu, L. Dai, J. Shui, Off/on switchable smart electromagnetic interference shielding aerogel, Matter 4 (2021) 1735–1747, https://doi.org/10.1016/j.matt.2021.02.022.

[7] Y. Tang, W. Dong, L. Tang, Y.K. Zhang, J. Kong, J. Gu, Fabrication and investigations on the polydopamine/KH-560 functionalized PBO fibers/cyanate ester wave-transparent composites, Compos. Commun. 8 (2018) 36–41, https://doi.org/10.1016/j.coco.2018.03.006.

[8] N. Yousefi, X. Sun, X. Lin, X. Shen, J. Jia, B. Zhang, B. Tang, M. Chan, J.K. Kim, Highly aligned graphene/polymer nanocomposites with excellent dielectric properties for high-performance electromagnetic interference shielding, Adv. Mater. 26 (2014) 5480–5487, https://doi.org/10.1002/adma.201305293.

[9] Y. Xia, W. Gao, C. Gao, A review on graphene-based electromagnetic functional materials: electromagnetic wave shielding and absorption, Adv. Funct. Mater. 32 (2022) 2204591, https://doi.org/10.1002/adfm.202204591.

[10] X. Zeng, X. Cheng, R. Yu, G.D. Stucky, Electromagnetic microwave absorption theory and recent achievements in microwave absorbers, Carbon 168 (2020) 606–623, https://doi.org/10.1016/j.carbon.2020.07.028.

[11] F. Ruiz-Perez, S.M. López-Estrada, R.V. Tolentino-Hernández, F. Caballero-Briones, Carbon-based radar absorbing materials: a critical review, J. Sci. Adv. Mater. Devices 7 (3) (2022), 100454, https://doi.org/10.1016/j.jsamd.2022.100454.

[12] Y. Liu, Y. Liu, M.G.B. Drew, A theoretical investigation of the quarter-wavelength model-part 2: verification and extension, Phys. Scr. 97 (1) (2022), 015806, https://doi.org/10.1088/1402-4896/ac1eb1.

[13] X. Li, L. Zhu, T. Kasuga, M. Nogi, H. Koga, Chitin-derived-carbon nanofibrous aerogel with anisotropic porous channels and defective carbon structures for strong microwave absorption, Chem. Eng. J. 450 (2022), 137943, https://doi.org/10.1016/j.cej.2022.137943.

[14] J.B. Kim, S.K. Lee, C.G. Kim, Comparison study on the effect of carbon nano materials for single-layer microwave absorbers in X-band, Compos. Sci. Technol. 68 (2008) 2909–2916, https://doi.org/10.1016/j.compscitech.2007.10.035.

[15] X. Peng, K. Wu, Y. Hu, H. Zhuo, Z. Chen, S. Jing, Q. Liu, C. Liu, L. Zhong, A mechanically strong and sensitive CNT/rGO-CNF carbon aerogel for piezoresistive sensors, J. Mater. Chem. A 6 (2018) 23550–23559, https://doi.org/10.1039/C8TA09322A.

[16] Y. Si, J. Yu, X. Tang, J. Ge, B. Ding, Ultralight nanofibre-assembled cellular aerogels with superelasticity and multifunctionality, Nat. Commun. 5 (2014) 5802, https://doi.org/10.1038/ncomms6802.

[17] S.S. Kim, S.B. Jo, K.I. Gueon, K.K. Choi, J.M. Kim, K.S. Churn, Complex permeability and permittivity and microwave absorption of ferrite-rubber composite in X-band frequencies, IEEE Trans. Magn. 27 (1991) 5462–5464, https://doi.org/10.1109/20.278872.

[18] Y. Naito, K. Suetake, Application of ferrite to electromagnetic wave absorber and its characteristics, IEEE Trans. Microw. Theory Tech. 19 (1971) 65–72, https://doi.org/10.1109/TMTT.1971.1127446.

[19] H. Xu, X. Yin, M. Zhu, M. Han, Z. Hou, X. Li, L. Zhang, L. Cheng, Carbon hollow microspheres with a designable mesoporous shell for high-performance electromagnetic wave absorption, ACS Appl. Mater. Interfaces 9 (2017) 6332–6341, https://doi.org/10.1021/acsami.6b15826.

[20] C. Tian, Y. Du, P. Xu, R. Qiang, Y. Wang, D. Ding, J. Xue, J. Ma, H. Zhao, X. Han, Constructing uniform core-shell PPy@PANI composites with tunable shell thickness toward enhancement in microwave absorption, ACS Appl. Mater. Interfaces 7 (2015) 20090–20099, https://doi.org/10.1021/acsami.5b05259.

[21] X. Li, L. Yu, L. Yu, Y. Dong, Q. Gao, Q. Yang, W. Yang, Y. Zhu, Y. Fu, Chiral polyaniline with superhelical structures for enhancement in microwave absorption, Chem. Eng. J. 352 (2018) 745–755, https://doi.org/10.1016/j.cej.2018.07.096.

[22] J. Huang, B.G. Sumpter, V. Meunier, Theoretical model for nanoporous carbon supercapacitors, Angew. Chem. Int. Ed. 47 (2008) 520–524, https://doi.org/10.1002/anie.200703864.

[23] A.K. Jonscher, The 'universal' dielectric response, Nature 267 (1977) 673–679. https://www.nature.com/articles/267673a0.

[24] S. Deville, E. Saiz, R.K. Nalla, A.P. Tomsia, Freezing as a path to build complex composites, Science 311 (2006) 515–518, https://doi.org/10.1126/science.1120937.

[25] K.H. Kim, Y. Oh, M.F. Islam, Graphene coating makes carbon nanotube aerogels superelastic and resistant to fatigue, Nat. Nanotechnol. 7 (2012) 562–566, https://doi.org/10.1038/nnano.2012.118.

[26] T.A. Schaedler, A.J. Jacobsen, A. Torrents, A.E. Sorensen, J. Lian, J.R. Greer, L. Valdevit, W.B. Carter, Ultralight metallic microlattices, Science 334 (2011) 962–965, https://doi.org/10.1126/science.1211649.
[27] L. Qiu, J.Z. Liu, S.L.Y. Chang, Y. Wu, D. Li, Biomimetic superelastic graphene-based cellular monoliths, Nat. Commun. 3 (2012) 1241, https://doi.org/10.1038/ncomms2251.
[28] C. Li, M. Ding, B. Zhang, X. Qiao, C.Y. Liu, Graphene aerogels that withstand extreme compressive stress and strain, Nanoscale 10 (2018) 18291–18299, https://doi.org/10.1039/c8nr04824j.
[29] L. Liang, Q. Li, X. Yan, Y. Feng, Y. Wang, H. Bin Zhang, X. Zhou, C. Liu, C. Shen, X. Xie, Multifunctional magnetic $Ti_3C_2T_x$MXene/graphene aerogel with superior electromagnetic wave absorption performance, ACS Nano 15 (2021) 6622–6632, https://doi.org/10.1021/acsnano.0c09982.
[30] C.M. Watts, X. Liu, W.J. Padilla, Metamaterial electromagnetic wave absorbers, Adv. Mater. 24 (23) (2012) OP98–OP120, https://doi.org/10.1002/adma.201200674.
[31] F. Pan, L. Cai, Y. Shi, Y. Dong, X. Zhu, J. Cheng, H. Jiang, X. Wang, Y. Jiang, W. Lu, Heterointerface engineering of β-chitin/carbon nano-onions/Ni–P composites with boosted maxwell-wagner-sillars effect for highly efficient electromagnetic wave response and thermal management, Nano-Micro Lett. 14 (2022) 85, https://doi.org/10.1007/s40820-022-00804-w.
[32] F. Pan, Y. Rao, D. Batalu, L. Cai, Y. Dong, X. Zhu, Y. Shi, Z. Shi, Y. Liu, W. Lu, Macroscopic electromagnetic cooperative network-enhanced MXene/Ni chains aerogel-based microwave absorber with ultra-low matching thickness, Nano-Micro Lett. 14 (2022) 140, https://doi.org/10.1007/s40820-022-00869-7.
[33] L. Cai, F. Pan, X. Zhu, Y. Dong, Y. Shi, Z. Xiang, J. Cheng, H. Jiang, Z. Shi, W. Lu, Etching engineering and electrostatic self-assembly of N-doped MXene/hollow Co-ZIF hybrids for high-performance microwave absorbers, Chem. Eng. J. 434 (2022), 133865, https://doi.org/10.1016/j.cej.2021.133865.
[34] J. Cheng, H. Jiang, L. Cai, F. Pan, Y. Shi, X. Wang, X. Zhang, S. Lu, Y. Yang, L. Li, Z. Xiu, J. Wang, H. Guo, W. Lu, Porous N-doped C/VB-group VS_2 composites derived from perishable garbage to synergistically solve the environmental and electromagnetic pollution, Chem. Eng. J. 457 (2022), 141208, https://doi.org/10.1016/j.cej.2022.141208.
[35] I. Choi, J.G. Kim, D.G. Lee, I.S. Seo, Aramid/epoxy composites sandwich structures for low-observable radomes, Compos. Sci. Technol. 71 (2011) 1632–1638, https://doi.org/10.1016/j.compscitech.2011.07.008.
[36] Y. Yang, L. Xia, T. Zhang, B. Shi, L. Huang, B. Zhong, X. Zhang, H. Wang, J. Zhang, G. Wen, Fe_3O_4@LAS/RGO composites with a multiple transmission-absorption mechanism and enhanced electromagnetic wave absorption performance, Chem. Eng. J. 352 (2018) 510–518, https://doi.org/10.1016/j.cej.2018.07.064.
[37] Y. Xie, S. Liu, K. Huang, B. Chen, P. Shi, Z. Chen, B. Liu, K. Liu, Z. Wu, K. Chen, Y. Qi, Z. Liu, Ultra-broadband strong electromagnetic interference shielding with ferromagnetic graphene quartz fabric, Adv. Mater. 34 (2022) 2202982, https://doi.org/10.1002/adma.202202982.
[38] P. Yi, H. Zou, Y. Yu, X. Li, Z. Li, G. Deng, C. Chen, M. Fang, J. He, X. Sun, X. Liu, J. Shui, R. Yu, MXene-reinforced liquid metal/polymer fibers via interface engineering for wearable multifunctional textiles, ACS Nano 16 (2022) 14490–14502, https://doi.org/10.1021/acsnano.2c04863.
[39] Y. Yu, P. Yi, W. Xu, X. Sun, G. Deng, X. Liu, J. Shui, R. Yu, Environmentally tough and stretchable mxene organohydrogel with exceptionally enhanced electromagnetic interference shielding performances, Nano-Micro Lett. 14 (2022) 77, https://doi.org/10.1007/s40820-022-00819-3.
[40] J. Li, Y. Zhang, X. Li, C. Chen, H. Zou, P. Yi, X. Liu, R. Yu, Oriented magnetic liquid metal-filled interlocked bilayer films as multifunctional smart electromagnetic devices, Nano Res. 16 (2023) 1764–1772, https://doi.org/10.1007/s12274-022-4843-z.
[41] F. Meng, H. Wang, W. Wei, Z. Chen, T. Li, C. Li, Y. Xuan, Z. Zhou, Generation of graphene-based aerogel microspheres for broadband and tunable high-performance microwave absorption by electrospinning-freeze drying process, Nano Res. 11 (2018) 2847–2861, https://doi.org/10.1007/s12274-017-1915-6.
[42] G. Ma, Y. Zeng, X. Yang, Y. Liu, Y. Duan, Wave-transmitting material to optimize impedance matching and enhance microwave absorption properties of flaky carbonyl iron coating, J. Mater. Sci-Mater. Electron. 31 (2021) 8627–8636, https://doi.org/10.1007/s10854-020-03398-4.
[43] C.P. Neo, V.K. Varadan, Optimization of carbon fiber composite for microwave absorber, IEEE Trans. Electromagn. Compat. 46 (2004) 102–106, https://doi.org/10.1109/TEMC.2004.823618.
[44] X.X. Wang, M. Zhang, J.C. Shu, B. Wen, W.Q. Cao, M.S. Cao, Thermally-tailoring dielectric “genes” in graphene-based heterostructure to manipulate electromagnetic response, Carbon 184 (2021) 136–145, https://doi.org/10.1016/j.carbon.2021.07.099.
[45] X. Qian, Y. Zhang, Z. Wu, R. Zhang, X. Li, M. Wang, R. Che, Multi-path electron transfer in 1D double-shelled Sn@Mo_2C/C tubes with enhanced dielectric loss for boosting microwave absorption performance, Small 17 (2021) 2100283, https://doi.org/10.1002/smll.202100283.